

## Solution structure of the N-terminal extension domain of a *Schistosoma japonicum* asparaginyl-tRNA synthetase

Yoshimi Peck<sup>a</sup>, Darren Pickering<sup>a</sup>, Mehdi Mobli<sup>b</sup>, Michael J. Liddell<sup>c</sup>, David T. Wilson<sup>a</sup>, Roland Ruscher<sup>a</sup>, Stephanie Ryan<sup>a</sup>, Geraldine Buitrago<sup>a,d</sup>, Connor McHugh<sup>a</sup>, Nicholas C. Love<sup>e</sup>, Theresa Pinlac<sup>f</sup>, Michael Haertlein<sup>g</sup>, Michael A. Kron<sup>h</sup>, Alex Loukas<sup>a</sup> and Norelle L. Daly<sup>a</sup>

<sup>a</sup>Australian Institute of Tropical Health and Medicine, James Cook University, Cairns, QLD, Australia; <sup>b</sup>Centre for Advanced Imaging, The University of Queensland, St Lucia, QLD, Australia; <sup>c</sup>College of Science and Engineering, James Cook University, Cairns, QLD, Australia; <sup>d</sup>Strathclyde Institute of Pharmacy and Biomedical Sciences, University of Strathclyde, Glasgow, UK; <sup>e</sup>Medical College of Wisconsin, Milwaukee, WI, USA; <sup>f</sup>Department of Biochemistry, University of the Philippines, Manila, Philippines; <sup>g</sup>Deuteration Laboratory, Institut Laue-Langevin, Grenoble, France; <sup>h</sup>Department of Medicine, Division of Infectious Diseases, Medical College of Wisconsin, Milwaukee, WI, USA

Communicated by Ramaswamy H. Sarma

### ABSTRACT

Several secreted proteins from helminths (parasitic worms) have been shown to have immunomodulatory activities. Asparaginyl-tRNA synthetases are abundantly secreted in the filarial nematode *Brugia malayi* (*BmAsnRS*) and the parasitic flatworm *Schistosoma japonicum* (*SjAsnRS*), indicating a possible immune function. The suggestion is supported by *BmAsnRS* alleviating disease symptoms in a T-cell transfer mouse model of colitis. This immunomodulatory function is potentially related to an N-terminal extension domain present in eukaryotic AsnRS proteins but few structure/function studies have been done on this domain. Here we have determined the three-dimensional solution structure of the N-terminal extension domain of *SjAsnRS*. A protein containing the 114 N-terminal amino acids of *SjAsnRS* was recombinantly expressed with isotopic labelling to allow structure determination using 3D NMR spectroscopy, and analysis of dynamics using NMR relaxation experiments. Structural comparisons of the N-terminal extension domain of *SjAsnRS* with filarial and human homologues highlight a high degree of variability in the  $\beta$ -hairpin region of these eukaryotic N-AsnRS proteins, but similarities in the disorder of the C-terminal regions. Limitations in PrDOS-based intrinsically disordered region (IDR) model predictions were also evident in this comparison. Empirical structural data such as that presented in our study for N-*SjAsnRS* will enhance the prediction of sequence-homology based structure modelling and prediction of IDRs in the future.

**Abbreviations:** AsnRS: Asparaginyl-tRNA synthetase; *SjAsnRS*: Asparaginyl-tRNA synthetase of *Schistosoma japonicum*; *BmAsnRS*: Asparaginyl-tRNA synthetase of *Brugia malayi*; *HsAsnRS*: Asparaginyl-tRNA synthetase of *Homo sapiens*; aaRSs: aminoacyl-tRNA synthetases; N-: N-terminal of; CXCR1: CXC chemokine receptor 1; CXCR2: CXC chemokine receptor 2; CCR3: CC chemokine receptor 3; 3D NMR: heteronuclear triple-resonance Nuclear Magnetic Resonance; HSQC: Heteronuclear Single Quantum Coherence; NOESY: Nuclear Overhauser Effect Spectroscopy; IDR: intrinsically disordered region

### ARTICLE HISTORY

Received 11 January 2023  
Accepted 24 July 2023

### KEYWORDS


$\beta$ -hairpin; tRNA synthetase; <sup>15</sup>N relaxation; 3D NMR; N-terminal extension; parasitic worm; intrinsically disordered region (IDR)


## 1. Introduction

Asparaginyl-tRNA synthetase (AsnRS) is a critical enzyme for both prokaryotes and eukaryotes because it catalyses the binding of asparagine to tRNA during protein translation (Ibba & Söll, 2000; Pang et al., 2014). In addition to this primary function, an immunomodulatory function has been identified for particular AsnRS proteins. Human AsnRS (*HsAsnRS*) is involved in the development of autoimmune diseases, such as interstitial lung disease or myositis (Park et al., 2018). In contrast, the AsnRS abundantly secreted by the helminth (parasitic worm) *Brugia malayi* (*BmAsnRS*) alleviates symptoms in a T-cell transfer mouse model of colitis (Kron et al., 2013).

*B. malayi* is classified as a filarial nematode, but immunomodulatory effects are not limited to this species and other types of helminths also produce proteins that have been shown to have immune-mediating effects (Ryan et al., 2020; Smallwood et al., 2017). Modulation of the immune responses of the mammalian hosts is thought to aid helminths to avoid expulsion and to establish long-term residence in the host (Maizels & McSorley, 2016; Nutman, 2015). In the context of drug discovery secreted helminth proteins also have considerable potential for the development of anti-inflammatory drug leads (Maizels et al., 2018; Ryan et al., 2020).

Most eukaryotic aminoacyl-tRNA synthetases have evolved an extension domain for a secondary function (Crepin et al.,

**CONTACT** Norelle L. Daly  norelle.daly@jcu.edu.au  Australian Institute of Tropical Health and Medicine, James Cook University, QLD, 4878, Australia

 Supplemental data for this article can be accessed online at <https://doi.org/10.1080/07391102.2023.2241918>.

© 2023 The Author(s). Published by Informa UK Limited, trading as Taylor & Francis Group  
This is an Open Access article distributed under the terms of the Creative Commons Attribution-NonCommercial-NoDerivatives License (<http://creativecommons.org/licenses/by-nc-nd/4.0/>), which permits non-commercial re-use, distribution, and reproduction in any medium, provided the original work is properly cited, and is not altered, transformed, or built upon in any way. The terms on which this article has been published allow the posting of the Accepted Manuscript in a repository by the author(s) or with their consent.

2011; Guo et al., 2010). In AsnRS proteins, an anti-codon binding domain and catalytic domain are conserved in both prokaryotic and eukaryotic AsnRS proteins, but the N-terminal extension domain is entirely absent in prokaryotic AsnRS proteins (Berthet-Colominas et al., 1998; Crepin et al., 2011; Guo et al., 2010; Rajendran et al., 2018) (Figure 1). Some eukaryotic N-terminal domains, including those in human and filarial AsnRS proteins, appear to be critical for the immunomodulatory function observed (Kron et al., 2012; Park et al., 2018). In *BmAsnRS*, the N-terminal extension domain alone (residues 1–111, N-*BmAsnRS*) induces chemotaxis towards neutrophils and eosinophils, while an analogue without the N-terminal domain (comprising residues 112–548) does not induce chemotaxis (Kron et al., 2012; Ramirez et al., 2006). Truncation studies on the human AsnRS have shown the N-terminal extension domain (residues 1–77, N-*HsAsnRS*) is involved in CC chemokine 3 receptor (CCR3)-mediated chemotactic activity for immune cells (Howard et al., 2002; Park et al., 2018).

Despite the potential significance of the N-terminal extension domain of AsnRS proteins, structural analyses of this domain have largely been overlooked. The currently available experimentally solved structures in the protein database are N-*BmAsnRS* (NMR, PDB 2KQR (Crepin et al., 2011)) and N-*HsAsnRS* (X-Ray, PDB 4ZYA (Park et al., 2018)). Both structures have the same secondary structure topology order  $\beta 1$ - $\alpha 1$ - $\beta 2$ - $\beta 3$ - $\alpha 2$  ( $\alpha 1$ : the first  $\alpha$ -helix,  $\beta 2$ : the second  $\beta$ -sheet) (Crepin et al., 2011; Park et al., 2018). An homology model (Phyre 2.0) for the N-AsnRS of the liver fluke *Fasciola gigantica* (N-*FgAsnRS*) (Rajendran et al., 2018) differs in the secondary structure topology order ( $\alpha 1$ - $\alpha 2$ - $\beta 1$ - $\beta 2$ - $\alpha 3$ ) and the location of disordered regions compared with the N-*BmAsnRS* and N-*HsAsnRS* structures.

To expand our knowledge of the N-terminal extension domain of AsnRS proteins, we have determined the three-dimensional (3D) structure of the N-terminal extension domain from the parasitic blood fluke *Schistosoma japonicum* AsnRS protein (N-*SjAsnRS*). Cytoplasmic *SjAsnRS* is one of the most abundantly secreted proteins of *S. japonicum* (Liu et al., 2009). Proteomics studies on this organism have identified several molecules with immunomodulatory effects (Liu et al., 2016; Shan et al., 2021; Sun et al., 2010; L. F. Wang et al., 2017; X. Wang et al., 2017; Zhang et al., 2019), but the effects of *SjAsnRS* have not been tested. We recombinantly expressed the 114 N-terminal residues of *SjAsnRS* (N-*SjAsnRS*) and determined the 3D structure using NMR spectroscopy and analysed the heteronuclear NOE, and longitudinal and transverse relaxation times. This structural analysis provides insight into both conserved and variable features in the eukaryote-specific N-terminal extension domain of this critical class of enzyme.

## 2. Methods

### 2.1. Expression and purification of recombinant N-terminal *SjAsnRS*

A recombinant form of N-*SjAsnRS* was expressed with  $^{13}\text{C}$  and  $^{15}\text{N}$  isotopic labelling in *Escherichia coli* using a method described elsewhere (Marley et al., 2001). Briefly, this involved cDNA encoding N-*SjAsnRS* with a hexa-histidine tag, which was then cloned into a pET30a vector and expressed in *E. coli* BL21 (DE3) cell culture. For isotopic labelling with  $^{13}\text{C}$  and  $^{15}\text{N}$ , cells were initially grown in LB broth with 50  $\mu\text{g}/\text{mL}$  kanamycin at 37 °C and agitated at 200 rpm. When the optical density at 600 nm ( $\text{OD}_{600}$ ) reached 0.7, the culture medium was replaced by M9 minimal growth media supplemented with Basal Vitamins Eagle media,  $\text{MgSO}_4$ ,  $\text{CaCl}_2$  and  $^{13}\text{C}$  D-glucose.  $\text{NH}_4\text{Cl}$  in the M9 media was substituted for isotopically labelled  $^{15}\text{NH}_4\text{Cl}$ . After one hour of incubation, protein expression was induced by isopropyl  $\beta$ -D-1-thiogalactopyranoside (IPTG) to a final concentration of 0.8 mM. The incubation time after induction was 4 h, before harvesting the cells (Marley et al., 2001). For the NMR relaxation experiments the protein was expressed with only  $^{15}\text{N}$  labelling, using similar methods without the use of  $^{13}\text{C}$  D-glucose.

BugBuster® Protein Extraction Reagent (Merck Pty. Ltd) was used to disrupt the cells and Immobilized Metal-Affinity Chromatography (IMAC, Cytiva) was used to isolate the target protein. The eluate, containing the target protein in imidazole buffer, was buffer-exchanged and concentrated into PBS (phosphate-buffered saline, 2.7 mM KCl, 1.5 mM  $\text{KH}_2\text{PO}_4$ , 137.9 mM NaCl, 8.1 mM  $\text{Na}_2\text{HPO}_4$ , pH 7.1) using centrifugal concentrators (Ultra-15 Centrifugal Filter Units, Amicon) by repeated centrifugation (20 min at 4 °C and 3700 g). A yield of approximately 3 mg protein from 100 mL of labelled culture media was obtained. Protein mass was confirmed by sodium dodecyl sulphate-polyacrylamide gel electrophoresis (SDS-PAGE). The protein concentration was determined using a Pierce™ BCA (bicinchoninic acid) Protein Assay Kit (ThermoFisher Scientific).

### 2.2. NMR spectroscopy and structural analysis

The isotopically labelled N-*SjAsnRS* protein sample in PBS (500  $\mu\text{L}$ ) was mixed with 50  $\mu\text{L}$   $\text{D}_2\text{O}$ . All NMR spectra used for structure determination were acquired on a 900 MHz AVANCE III NMR spectrometer (Bruker, Karlsruhe, Germany) at 298 K (with a cryogenically cooled probe) with an inter-scan delay of 1 s. All 3D spectra, excluding NOESY experiments, were acquired using non-uniform sampling and processed using the Rowland NMR Toolkit (Mobli et al.,

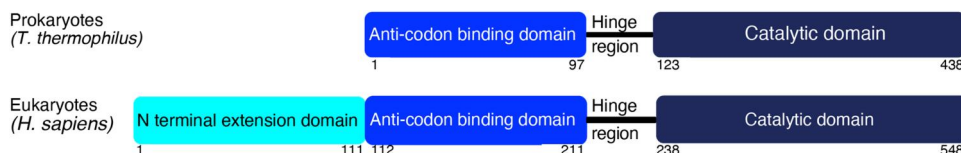


**Figure 1.** Comparison of the domain arrangement of prokaryotic and eukaryotic AsnRS proteins. Asparaginyl-tRNA synthetase proteins in prokaryotic species, such as *Thermus thermophilus*, consist of an anti-codon binding domain, catalytic domain and the hinge region between the domains. In eukaryotic species, such as *H. sapiens*, *B. malayi*, *F. gigantica* and *S. japonicum*, homologous proteins contain an additional N-terminal extension domain.

2007) and analysed using the CcpNmr software package (Vranken et al., 2005). The following methods, 2D  $^1\text{H}$ - $^{15}\text{N}$  HSQC, 3D HNCACB, 3D CBCA(CO)NH, and 3D HNCO spectra, were used for backbone sequence assignment, and 3D HBHA(CO)ONH, 3D CC(CO)NNH and 3D H(CCCO)NNH were used for side chain assignment (Ikura et al., 1990; Kay et al., 1990). Following backbone assignments, secondary chemical shifts were calculated by subtracting random coil shifts from the  $\text{H}\alpha$  shift (Wishart et al., 1995). NOESY spectra including 3D  $^{15}\text{N}$  NOESY-HSQC,  $^{13}\text{C}$ -aliphatic NOESY-HSQC and  $^{13}\text{C}$ -aromatic NOESY-HSQC with mixing times of 120 ms, were used to derive distance restraints.  $\varphi$  and  $\psi$  backbone torsion-angle restraints, protein backbone dynamics and secondary structures were predicted using TALOS-N (Shen et al., 2009; Shen & Bax, 2013), based on the chemical shift assignments of HN,  $\text{H}\alpha$ ,  $\text{C}\alpha$ ,  $\text{C}\beta$  resonances (Berjanskii & Wishart, 2005; 2007; 2008). Initial structures were calculated using the CYANA program incorporating the TALOS-N angle restraints, and distance restraints based on automatic assignment of the NOESY spectra (Guntert, 2004). The TALOS-N derived angle restraints, and interproton distance restraints derived from CYANA were subsequently used in CNS structure calculations with refinement in explicit water using scripts previously described (Brünger et al., 1998; Nederveen et al., 2005). A set of 20 structures with the lowest energy, no violations greater than  $0.5 \text{ \AA}$  or  $4^\circ$  (distance or angle violation, respectively), were selected for the final ensemble. Structure quality was analysed using PSVS (Bhattacharya et al., 2007), and structures were visualised using MOLMOL (Koradi et al., 1996).

### 2.3. NMR relaxation experiments

To study the backbone motion of N-SjAsnRS,  $\{^1\text{H}\}$ - $^{15}\text{N}$  Nuclear Overhauser effects (NOEs), and longitudinal ( $R_1$ ) and transverse ( $R_2$ ) relaxation rates were measured on a 600 MHz Bruker spectrometer equipped with a cryoprobe. Data were acquired at 298 K on a 0.1 mM sample of  $^{15}\text{N}$  labelled N-SjAsnRS.  $\{^1\text{H}\}$ - $^{15}\text{N}$  heteronuclear NOEs were acquired with a relaxation delay of 5 s.  $T_1$  spectra were recorded with delays of 20, 60, 200, 600, 800, 1100, 1400 and 1800 ms. The 60 ms and 600 ms delays were repeated to ensure reproducibility of the results.  $T_2$  spectra were recorded with delay times of 16, 32, 64, 128, 160, 192, 224 and 256 ms. The 32 and 160 ms delays were repeated. Spectra were processed using the Rowland NMR toolkit (Mobli et al., 2007) and analysed using CcpNMR (Vranken et al., 2005).  $\{^1\text{H}\}$ - $^{15}\text{N}$  heteronuclear NOE values were determined by a ratio of cross-peak intensities with or without  $^1\text{H}$  saturation.  $^1\text{H}$ - $^{15}\text{N}$  HSQC spectra were recorded between the NOE,  $R_1$  and  $R_2$  experiments to ensure the sample had not degraded.

### 2.4. Prediction of IDR from sequence

The intrinsically disordered regions (IDRs) of N-SjAsnRS were predicted by using a sequence-based prediction tool (PrDOS: Protein DisOrder prediction System) (Ishida & Kinoshita, 2007), and the location of the disordered region was then

compared with the experimentally determined N-SjAsnRS structure.

## 3. Results

### 3.1. Isotopically labelled protein expression and purification of N-SjAsnRS

A recombinant form of N-SjAsnRS, expressed with  $^{13}\text{C}$  and  $^{15}\text{N}$  isotopic labelling in *E. coli*, had a single band at an approximate molecular weight of 14.3 kDa in SDS-PAGE gel, confirming expression of the protein and illustrating the purity (Supplementary Figure S1). The isolated fraction was buffer exchanged and concentrated for NMR experiments.

### 3.2. Description of the overall structure of N-SjAsnRS

Initial analysis of the 2D  $^1\text{H}$ - $^{15}\text{N}$  HSQC spectrum (Supplementary Figure S2), recorded at a concentration of approximately 0.1 mM, indicated a well-defined structure for part of the protein based on the chemical shift dispersion but there was also significant overlap for several peaks. Analysis of the suite of NMR spectra collected allowed the majority of the backbone assignments to be made, but several residues, including Gln2, Ala14, Pro22, Ser59, Lys77, Pro79, His80, Glu81, Glu84 and Pro109, could not be assigned.

Analysis of the secondary chemical shifts (Supplementary Figure S3A) and secondary structure probabilities from TALOS-N (Figure 2A) indicates the presence of several  $\beta$ -sheets and helices in the N-terminal region (residues 1 to 73) in contrast to the C-terminal region of N-SjAsnRS (residues 74–114), where the secondary shifts are close to random coil (Supplementary Figure S3B) and no secondary structure was predicted. Furthermore, the random coil index-order parameters ( $\text{RCI-S}^2$ ) predicted from TALOS-N are consistent with the C-terminal region being dynamic (Figure 2B). The backbone NH peaks of the well-structured region (residues 1–73) are highlighted in black, and the overlapped backbone NH peaks of the disordered region (residues 74–114) are highlighted in red, in the 2D  $^1\text{H}$ - $^{15}\text{N}$  HSQC spectrum (Supplementary Figure S2).

Calculation of the three-dimensional structures of N-SjAsnRS with water refinement in CNS (the PDB and BMRB codes are 8FA3 and 31060, respectively) confirmed a well-defined region for residues 1–73, followed by a disordered region comprising residues 74–114. The well-defined region has a backbone RMSD of  $0.97 \pm 0.27 \text{ \AA}$  (Table 1) and contains two  $\alpha$ -helices and three  $\beta$ -strands in the order of  $\beta_1$ - $\alpha_1$ - $\beta_2$ - $\beta_3$ - $\alpha_2$ . The  $\beta_1$  and  $\beta_2$  strands are parallel while  $\beta_2$  and  $\beta_3$  are in an antiparallel orientation (Figure 3). The 20 conformers with the lowest energy are shown in Supplementary Figure S4, and the structure with the lowest energy is displayed in Figure 3. The structural statistics for the final ensemble of structures are shown in Table 1.

The secondary structure is consistent with the secondary structure probabilities (Figure 2A) and secondary chemical shift analysis (Supplementary Figure S3A). Glu19 has significantly shielded  $\alpha$  and  $\beta$  protons, which is supported by close

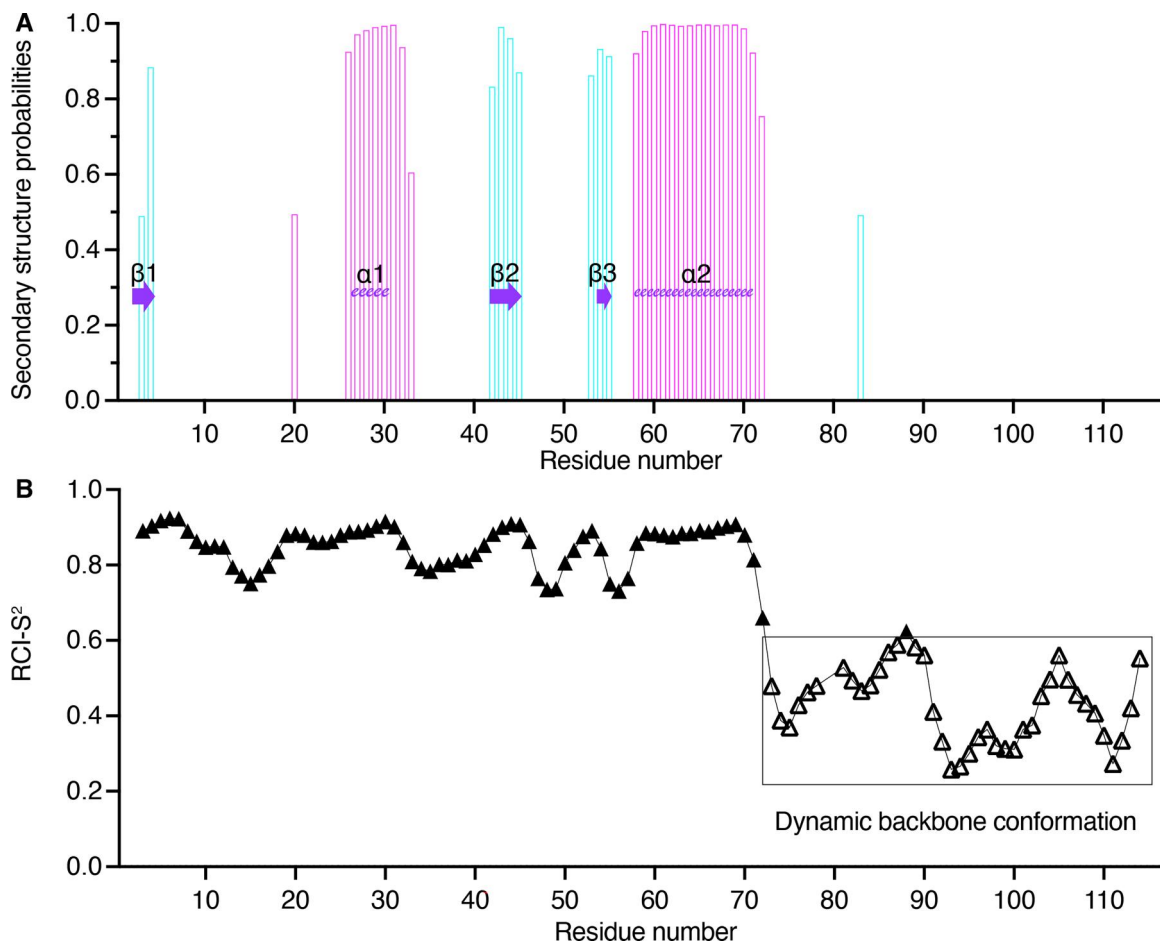


**Figure 2.** Secondary structure probabilities and local order parameters predicted from TALOS-N for N-SjAsnRS. (B) Random coil Index-Order parameters (RCI-S<sup>2</sup>). The C-terminal region has lower order parameters and is predicted to be dynamic. This region is highlighted with a box and open triangles. A threshold of RCI-S<sup>2</sup> < 0.6 was used to consider a residue dynamic. (A) The secondary structure probabilities of N-SjAsnRS. The height of the bar indicates the probability of the secondary structure.  $\alpha$ -helices are in magenta,  $\beta$ -strands are in cyan. The secondary structures present in our NMR structure are indicated by purple arrows and spirals.  $\alpha 1$  = alpha-helix 1.  $\beta 1$  = beta-strand 1.

interactions with Trp53 and Tyr4 in the three-dimensional structures. Aromatic residues are known to cause significant chemical shift perturbations of neighbouring residues. The disordered region between residues 74–114 has a backbone RMSD of  $11.64 \pm 3.31$  Å. Although the disordered structure results from the lack of restraints in this region, it is likely this region of the protein is flexible in solution based on the chemical shifts being close to random coil (Supplementary Figure S3B), the lack of NOE peaks and the local order parameters (RCI-S<sup>2</sup>) predicted from TALOS-N (Figure 2B). Furthermore, the NMR-derived structure for the related protein, N-BmAsnRS, also has disorder in this region (Crepin et al., 2011). To experimentally confirm the presence of disorder for the C-terminal residues 74–114, <sup>15</sup>N relaxation experiments were conducted.

### 3.3. Heteronuclear relaxation experiments

Relaxation of <sup>15</sup>N amide nuclei allowed us to characterise the protein backbone mobility in solution (Kay et al., 1989; Kharchenko et al., 2020; Rahnama et al., 2017; Saez et al., 2011). <sup>1</sup>H}-<sup>15</sup>N NOEs, R<sub>1</sub> and R<sub>2</sub> relaxation rates, which are relaxation parameters commonly used to investigate the protein backbone motion (Kharchenko et al., 2020), were

acquired for the backbone <sup>15</sup>N nuclei of N-SjAsnRS (Figure 4). Thirty seven out of 114 residues were not included in the relaxation analysis due to low signal to noise ratio and overlapping peaks. <sup>1</sup>H}-<sup>15</sup>N heteronuclear NOE values were determined to identify fast protein backbone motion (Gong & Ishima, 2007; Kharchenko et al., 2020; Palmer, 1997; Rahnama et al., 2017). There were significant differences in the <sup>1</sup>H}-<sup>15</sup>N heteronuclear NOEs between the N-terminal (residues 1–73) and C-terminal (residues 74–114) regions of N-SjAsnRS, with average values of  $0.73 \pm 0.063$  and  $-0.13 \pm 0.062$ , respectively. This difference indicates that the backbone motion is distinct between the two regions. The experimentally acquired negative NOE values suggest that the C-terminal region is disordered (Rahnama et al., 2017). In contrast, the elevated NOE values (close to one) indicates that N-terminal region is more rigid than the C-terminal region. There is a clear difference in the R<sub>2</sub>/R<sub>1</sub> ratio between the N-terminal (residues 1–73) and C-terminal (residues 74–114) regions (average  $6.60 \pm 1.03$  and  $2.38 \pm 0.41$ , respectively). The residues with higher R<sub>2</sub>/R<sub>1</sub> ratio coincide with the well-structured region while residues with lower ratio are found in the disordered region consistent with distinct differences in the backbone motions between the two regions (Figure 4).

**Table 1.** Statistics and analysis of the N-SjAsnRS protein structure.

Structural statistics of the N-SjAsnRS protein	
Experimental restraints	
Interproton distance restraints	
Intraresidue	300
Sequential	404
Medium range ( $i-j < 5$ )	197
Long range ( $i-j \geq 5$ )	233
Total	1134
Dihedral-angle restraints <sup>a</sup>	128
Restraint statistics	
Average number of violations per structure <sup>b</sup>	
NOE restraints $>0.5 \text{ \AA}$	0
Dihedral restraints $>4^\circ$	0
RMS of violations <sup>b</sup>	
NOE restraints ( $\text{\AA}$ )	$0.018 \pm 0.0011$
Dihedral restraints ( $^\circ$ )	$0.68 \pm 0.14$
RMS from idealised covalent geometry <sup>b</sup>	
RMS for bond length ( $\text{\AA}$ )	$0.0033 \pm 0.00013$
RMS for bond angles ( $^\circ$ )	$0.46 \pm 0.017$
RMS for impropers ( $^\circ$ )	$0.43 \pm 0.021$
Structural quality (ordered residues <sup>*</sup> )	
RMSD from average structure ( $\text{\AA}$ ) <sup>c</sup>	
Backbone atoms	$0.97 \pm 0.27$
Heavy atoms	$1.64 \pm 0.32$
Ramachandran statistics (%) <sup>d</sup>	
Most favoured regions	89.4
Additionally allowed regions	10.6
Generously allowed regions	0.0
Disallowed regions	0.0
Global quality scores (raw/Z scores) <sup>d</sup>	
Verify3D	0.13/-5.30
ProsaII (-ve)	0.26/-1.61
PROCHECK (all)	-0.46/-2.72
MolProbity clashscore	16.09/-1.24

<sup>a</sup>Predicted from TALOS-N (Shen et al., 2009; Shen & Bax, 2013).

<sup>b</sup>Derived from CNS (Brünger et al., 1998).

<sup>c</sup>Calculated using MOLMOL (Koradi et al., 1996).

<sup>d</sup>Evaluated by PSVS (Bhattacharya et al., 2007).

<sup>\*</sup>Ordered residue ranges: Residues 2–46, 50–72 are selected based on sum of  $\varphi$  and  $\psi$  order parameter  $\geq 1.8$  (PSVS).

### 3.4. IDR prediction of N-SjAsnRS

PrDOS was used to predict any IDR in N-SjAsnRS and the predicted results compared to the experimentally determined structure of N-SjAsnRS (Figure 5). Our experimentally acquired relaxation data (Figure 4), NMR structure (Figure 3), the secondary shifts analysis (Supplementary Figure S3B), and the RCI-S<sup>2</sup> local order parameter prediction (Figure 2B) indicated that the C-terminal region between residues 74–114 is unstructured (or disordered) in solution. The predicted results from PrDOS also suggested that the C-terminal residues 70–91 and 107–114 are intrinsically disordered in N-SjAsnRS (Figure 5).

Somewhat surprisingly, residues 92–106 were not predicted to be disordered, but there is no evidence from the <sup>15</sup>N relaxation parameters (Figure 4), angle or distance restraints based on the NMR data (Figure 3) to support this region having structure. In addition, the N-terminal residues 1–18 of N-SjAsnRS were predicted to be disordered (Figure 5) but this region of the NMR-derived structures is well defined, and includes a  $\beta$ -strand (Figure 3; Supplementary Figure S4). The lack of disorder in this region is supported by experimentally acquired relaxation data (Figure 4) and the

chemical shifts of residues 1–25 which are mostly larger than 0.1 ppm relative to random coil shifts (supplementary Figure S3A). Thus, multiple discrepancies were found in the IDR prediction of the structural characteristics of N-SjAsnRS.

### 3.5. Comparison of N-AsnRS structures

The amino acid sequence of N-SjAsnRS was aligned with that of N-BmAsnRS, N-HsAsnRS and N-FgAsnRS in Figure 6 (Crepin et al., 2011; Park et al., 2018; Rajendran et al., 2018) to identify conserved sequence in this domain. Intriguingly, sequence conservation was found in the unstructured region (residues 92–108) while the sequence around the second  $\beta$ -strand ( $\beta_2$ ) in the well-defined region was not conserved.

Pairwise sequence alignment of the N-SjAsnRS with each eukaryotic N-AsnRS was performed (Supplementary Figure S5). Despite high sequence homology between N-SjAsnRS and N-FgAsnRS (over 80% in the well-defined region), the NMR-derived structure of N-SjAsnRS was not similar to the predicted structure of N-FgAsnRS, but similarities were found with both human and filarial AsnRS proteins. A comparison of the secondary structure of N-SjAsnRS with the experimental structures of N-BmAsnRS (Crepin et al., 2011) and N-HsAsnRS (Park et al., 2018), and the modelled structure of N-FgAsnRS (Rajendran et al., 2018) is shown in Figure 7. Only the first approximately 70 residues have regular secondary structure. The secondary structure arrangement for all experimental structures, including N-SjAsnRS, N-BmAsnRS and N-HsAsnRS, are  $\beta_1$ - $\alpha_1$ - $\beta_2$ - $\beta_3$ - $\alpha_2$  (two  $\alpha$ -helices and three  $\beta$ -strands). In contrast, the modelled structure of N-FgAsnRS has the secondary structure arrangement in the order of  $\alpha_1$ - $\alpha_2$ - $\beta_1$ - $\beta_2$ - $\alpha_3$  (consisting of three  $\alpha$ -helices and two  $\beta$ -strands).

There are distinctions in the disordered regions as well (Figure 7). The NMR derived structures for N-SjAsnRS and N-BmAsnRS show disorder for residues 74–114 and 76–111, respectively. It is not clear if the equivalent region in N-HsAsnRS is disordered as the crystal structure only contained residues 4–77. In contrast, the modelled structure of N-FgAsnRS was predicted to have two unstructured regions (residues 1–15 and residues 81–112), which conflicts with the experimental structures which have demonstrated the presence of a  $\beta$ -strand,  $\beta_1$  (Crepin et al., 2011; Park et al., 2018; Rajendran et al., 2018) in residues 1–15 (Figure 7). Thus, multiple discrepancies were observed between the modelled structure of N-FgAsnRS and experimentally determined structures, including the new solution structure with relaxation properties for N-SjAsnRS.

It has previously been highlighted that the major structural difference between N-BmAsnRS and N-HsAsnRS (Park et al., 2018) is in a region corresponding to a  $\beta$ -hairpin. In this study both the 3D structures (the  $\beta$ -hairpin is highlighted in Figure 8A) and sequence comparisons (Figure 8B) have confirmed the distinction between structures in the N-terminal extension domain of AsnRS proteins is primarily in this  $\beta$ -hairpin region (i.e. N-SjAsnRS, N-Bm-AsnRS and N-HsAsnRS). The length of the  $\beta$ -strands, the size of the loops and the charge distribution varies amongst the three species. The negatively charged acidic residues dominate the

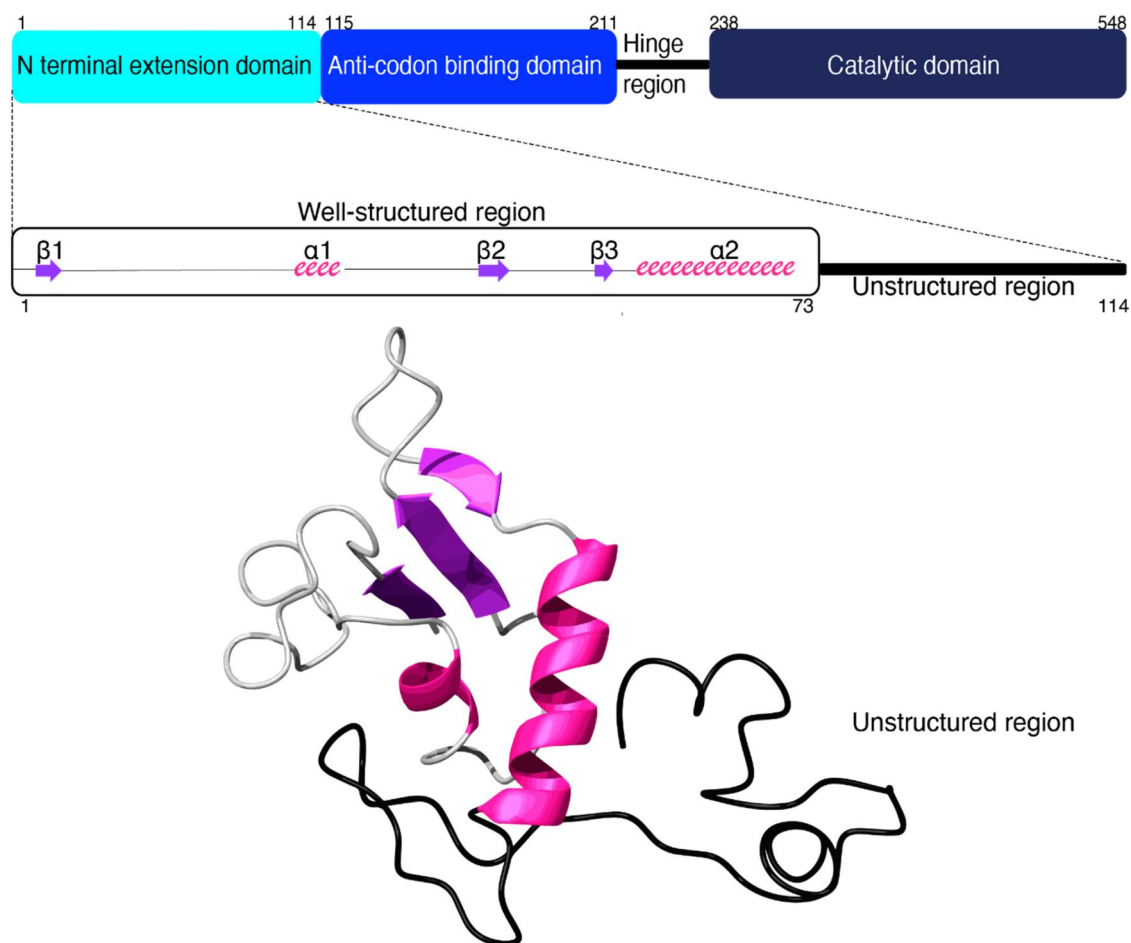


**Figure 3.** The domain arrangement of *SjAsnRS* and the solution NMR 3D structure of N-*SjAsnRS*. In the well-structured region (residues 1–73) pink spirals represent  $\alpha$ -helices and purple arrows represent  $\beta$ -strands. The unstructured region comprising residues 74–114 is shown in black. The domain arrangements and schematic representation of the secondary structure are shown at the top of the figure.

$\beta$ -hairpin region of N-*SjAsnRS* while N-*BmAsnRS* and N-*HsAsnRS* contain both positively and negatively charged residues (Figure 8B). The presence of methionine, which can form non-covalent interactions with aromatic residues to stabilise receptor-ligand interactions (Imai et al., 2007; Valley et al., 2012), is also unique to N-*SjAsnRS*.

#### 4. Discussion

The significance of the N-terminal extension domain of the eukaryotic AsnRS protein has been highlighted in human and filarial AsnRS (Kron et al., 2012; Park et al., 2018). However, there has been limited structural analyses on domains from other species. To explore this rather overlooked domain, we have determined the structure and relaxation properties of the N-terminal extension domain of the AsnRS from the blood fluke, *S. japonicum*.

The NMR structure revealed the first 73 residues of N-*SjAsnRS* fold into a well-defined structure in contrast to residues 74–114 which were disordered. The presence of the unstructured region was supported by subsequent NMR relaxation experiments. The heteronuclear NOE data and  $R_2/R_1$  ratio suggested that the backbone molecular motion is distinct between the well-structured and disordered region. Although the heteronuclear NOE values (Figure 4) for the

first 73 residues are considerably higher than the C-terminal region, the loops between the  $\alpha 1$  and  $\beta 2$ , and  $\beta 2$  and  $\beta 3$  have slightly lower values indicating that these loops are more flexible than the secondary structure elements. Overall, the relaxation experiments are consistent with the secondary chemical shift analysis (Supplementary Figure S3A and S3B), and the RCI- $S^2$  local order parameter prediction (Figure 2B). Furthermore, the location of the unstructured region of our N-*SjAsnRS* is consistent with the NMR structure of N-*BmAsnRS* (Crepin et al., 2011). The X-ray structure of *HsAsnRS* (Park et al., 2018) was determined on a construct containing residues 4–77 because a construct containing the whole N-terminal domain (residues 1–115) could not be crystallised (Park et al., 2018). It appears likely that the inability of crystals to form for the whole N-terminal domain is related to disorder for 78–115.

The biological role of this unstructured region in AsnRS proteins is still unclear. It has previously been suggested that this region forms a flexible linker between the two major domains to facilitate tRNA binding (Crepin et al., 2011) or to ensure that the N-terminal extension domain is conformationally independent (Yang, 2013). However, given the sequence conservation in residues 92–108 (Figure 6), this unstructured region may be more than a flexible linker, and could potentially share a common function across the

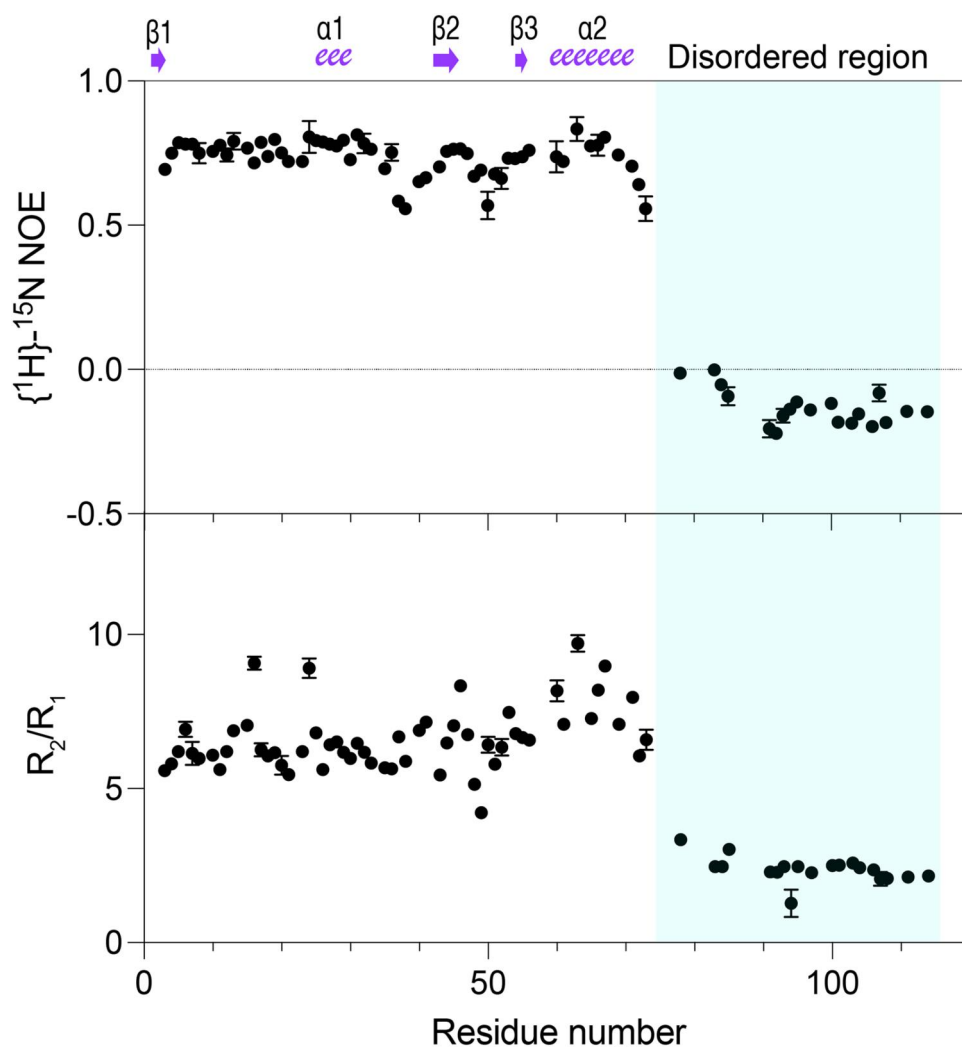


**Figure 4.**  $^1\text{H}$ - $^{15}\text{N}$  steady state NOE and ratio of longitudinal ( $R_1$ ) and transverse ( $R_2$ ) relaxation rates ( $R_2/R_1$ ) for N-SjAsnRS. Data was acquired on a 600 MHz Bruker spectrometer equipped with a cryoprobe at 298 K on a 100  $\mu\text{M}$  sample of  $^{15}\text{N}$  labeled N-SjAsnRS. The errors in the  $\{^1\text{H}\}$ - $^{15}\text{N}$  steady state NOE are a function of the S/N in the acquired spectra and the errors in  $R_1$  and  $R_2$  are time constant errors. Thirty-seven out of 114 residues were not included in the relaxation analysis due to low signal to noise ratio or overlapping peaks. The secondary structure is schematically represented at the top of the diagram.

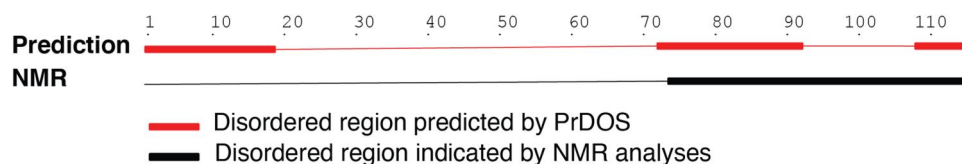


**Figure 5.** Predicted disordered regions in N-SjAsnRS. The thick red line represents disordered regions predicted by PrDOS (Ishida & Kinoshita, 2007) whereas the thick black line represents the disordered region indicated by NMR analyses. The residue numbers are indicated on the top of the figure. The prediction suggests the disorder is not continuous in the C-terminal region, in contrast to the experimentally derived three-dimensional structure.

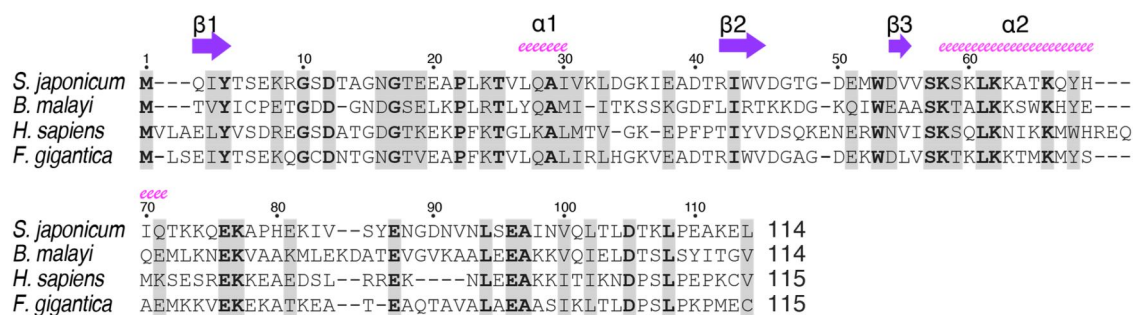


**Figure 6.** Sequence alignment of the N-terminal extension domain of AsnRS protein from four eukaryotic species. Conserved residues (defined as either identical or similar residues), are shaded in grey. Identical residues are also highlighted in bold. Secondary structures of N-SjAsnRS are shown above its sequence. Pink spirals represent  $\alpha$ -helices and purple arrows represent  $\beta$ -strands.

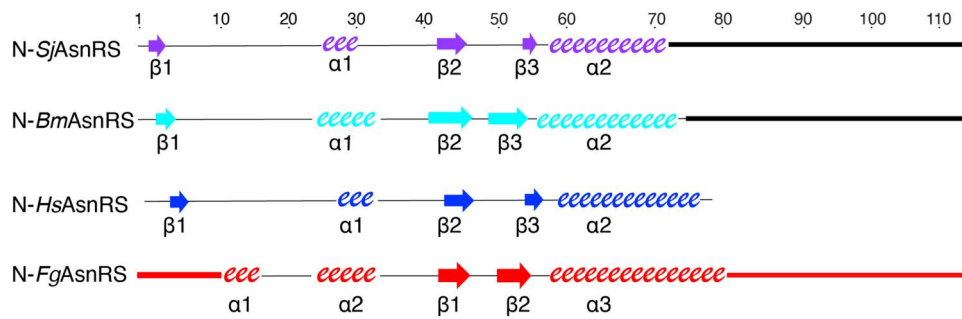


**Figure 7.** Comparison of the secondary structures in the N-terminal extension domain of AsnRS from four eukaryotic species. The  $\alpha$ -helices,  $\beta$ -strands and unstructured regions present in N-SjAsnRS, N-BmAsnRS, N-HsAsnRS, and N-FgAsnRS are represented with spirals, arrows and thick lines respectively. The crystal structure of N-HsAsnRS (PDB 4ZYA (Park et al., 2018) only contains residues 4–77; therefore residues after 78 are not included in the figure. Overall, the secondary structure is similar, with the main differences at the N-terminus of the domain.

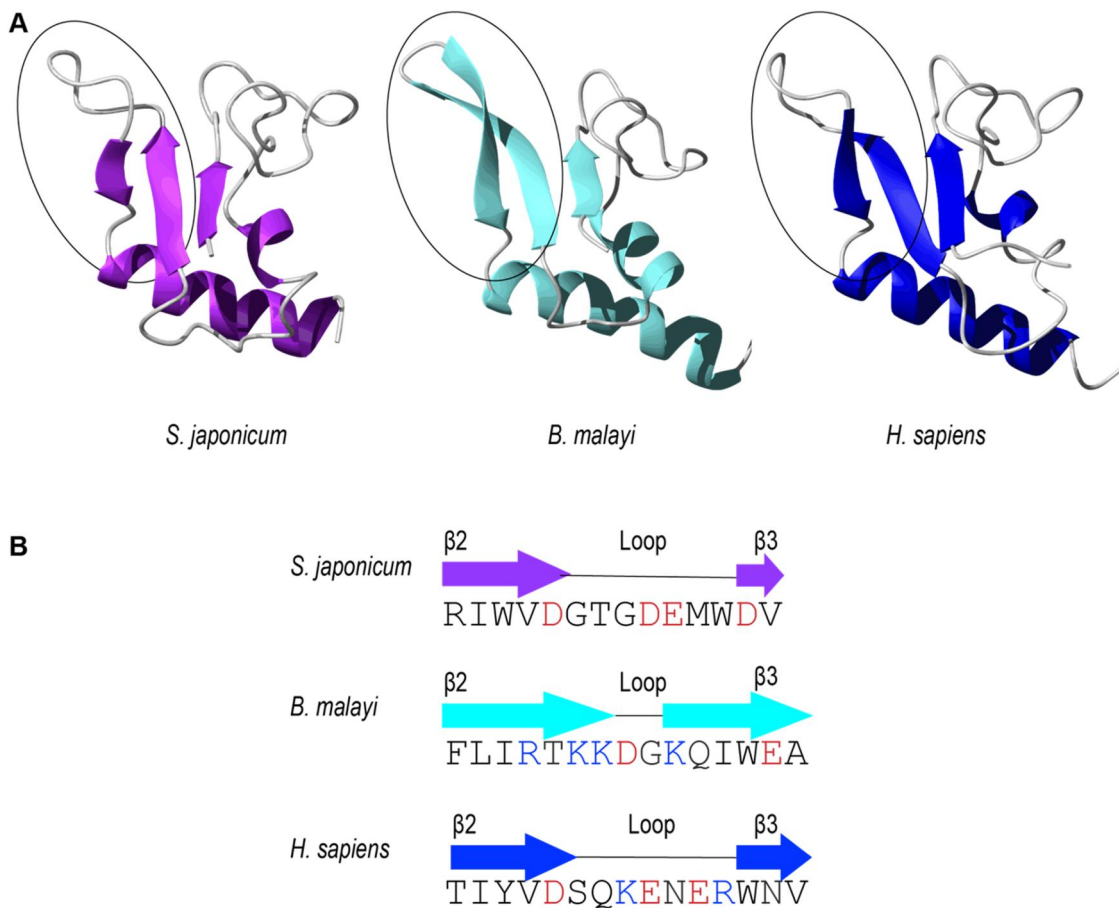


**Figure 8.** (A) Structural comparison of the  $\beta$ -hairpin region of AsnRS from three eukaryotic species. Only the well-structured region is displayed, residues 1–73 for *S. japonicum*, residues 1–75 for *B. malayi* and residues 1–77 for *H. sapiens*. The  $\beta$ -hairpin region is circled with a black line. (B) Sequence comparison of the  $\beta$ -hairpin region of AsnRS from three eukaryotic species. The location of  $\beta$ -strands ( $\beta 2$  and  $\beta 3$ ) and the loop is shown above the amino acid sequence. Positively charged residues are shown in blue, negatively charged residues are shown in red.

eukaryotic species. A recent study suggested a tendency for some IDRs to share conserved sequences, conserved disorder, and conserved functions (Zhou et al., 2019). PrDOS has been evaluated as one of the best performing IDR prediction tools in multiple studies (Deng et al., 2012; Liu et al., 2019; F. Meng et al., 2017; Fanchi Meng et al., 2017; Monastyrskyy et al., 2014). However, discrepancies were found in the PrDOS prediction compared to our experimentally acquired relaxation data and NMR structure (Figure 5). This potentially highlights the difficulty in predicting relatively long disordered regions in this critical class of enzyme.

Our structural and sequential comparison (Figure 8A and B) found variabilities in the  $\beta$ -hairpin region, which was suggested to be a part of the receptor-ligand interface in the studies of the human and filarial homologues (Kron et al., 2012; Park et al., 2018). These differences have been suggested to influence receptor binding (Park et al., 2018). In addition to significant conformational differences (i.e. loop size and length of strands), the prevalence of negatively charged acidic residues (Glu51, Asp46, Asp50 and Asp54) and the presence of methionine (Met52) are found to be unique to N-SjAsnRS (Figure 8B). These residues may play



key roles in non-covalent interactions, such as electrostatic interactions or a sulfur-aromatic interaction, in the receptor-ligand interface (Imai et al., 2007; Orabi & English, 2016; Valley et al., 2012; Zhou & Pang, 2018). The target receptor of N-SjAsnRS is still unknown but it appears the physiochemical differences in the  $\beta$ -hairpin region may affect the binding specificity (Kron et al., 2012; Park et al., 2018). Our current study on N-SjAsnRs indicated possible flexibility of the loop within the  $\beta$ -hairpin but further study on the dynamics of the related proteins might provide more insight into the structural differences between these proteins.

Pairwise alignment of the N-terminal extension of AsnRS (Supplementary Figure S5) suggests that the sequence of N-SjAsnRS has greater similarity to human compared to the filarial nematode protein, which does not align with general evolutionary understanding. Further investigation of sequence-structure-function relationship is warranted to determine the implications for this somewhat unexpected sequence alignment.

Anti-infective drugs targeting pathogen AsnRS and other aminoacyl-tRNA synthetases (aaRSs) have been explored based on structural differences between pathogen and human host aaRSs (Francklyn & Mullen, 2019; Laupland & Conly, 2003; Rock et al., 2007; Saint-Léger et al., 2016). These differences make it possible to inhibit the pathogen aaRSs without inhibiting the human enzymes (Nyamai & Tastan Bishop, 2019; O'Dwyer et al., 2015; Pham et al., 2014). However, aaRSs of various pathogens (from bacteria to the malaria causing parasite) have been reported to develop drug resistance (Bilsland et al., 2016; Francklyn & Mullen, 2019; Randall et al., 2016; Saint-Léger et al., 2016). The structural understanding developed in this study may help to overcome this challenge and design better aaRS inhibitors. For example, *Bm*AsnRS is a target for antiparasitic drug design and recent mutational studies of *Bm*AsnRS have suggested that the sites of mutation that confer drug resistance are likely to be around the  $\beta$ -hairpin and the second  $\alpha$ -helix region in the N-terminal extension domain (Chandrasekar et al., 2021). Thus, the significance of exploring the N-terminal extension domain of this class of enzyme is of major importance across multiple research areas.

In summary, we have shown a high degree of variability in the  $\beta$ -hairpin region of three eukaryotic N-AsnRS proteins, which warrants further functional studies. We have presented some inconsistencies in the molecular dynamics modelled structure of N-FgAsnRS with the three experimental structures and have found limitations in PrDOS-based IDR predictions. Information from experimentally verified IDRs can improve the performance of prediction tools (Liu et al., 2019; F. Meng et al., 2017). Thus, the structural data, including relaxation properties, reported here for N-SjAsnRS will assist in the development of better sequence-homology based structure modelling and prediction of IDRs in the future.

## Acknowledgments

The authors thank Dr Michael Smout and Dr Vignesh Ambothi Rathinasamy for assistance in the AITHM laboratory.

## Disclosure statement

No potential conflict of interest was reported by the author(s).

## Funding

Y.P was supported by a James Cook University Postgraduate Research Scholarship (JCUPRS). The James Cook University NMR facility was partially funded by the Australian Research Council (N.L.D., A.L.) (LE160100218).

## References

- Berjanskii, M. V., & Wishart, D. S. (2005). A simple method to predict protein flexibility using secondary chemical shifts. *Journal of the American Chemical Society*, 127(43), 14970–14971. <https://doi.org/10.1021/ja054842f>
- Berjanskii, M. V., & Wishart, D. S. (2007). The RCI server: Rapid and accurate calculation of protein flexibility using chemical shifts. *Nucleic Acids Research*, 35(Web Server issue), W531–537. <https://doi.org/10.1093/nar/gkm328>
- Berjanskii, M. V., & Wishart, D. S. (2008). Application of the random coil index to studying protein flexibility. *Journal of Biomolecular NMR*, 40(1), 31–48. <https://doi.org/10.1007/s10858-007-9208-0>
- Berthet-Colominas, C., Seignovert, L., Härtlein, M., Grotli, M., Cusack, S., & Leberman, R. (1998). The crystal structure of asparaginyl-tRNA synthetase from *Thermus thermophilus* and its complexes with ATP and asparaginyl-adenylate: The mechanism of discrimination between asparagine and aspartic acid. *The EMBO Journal*, 17(10), 2947–2960. <https://doi.org/10.1093/emboj/17.10.2947>
- Bhattacharya, A., Tejero, R., & Montelione, G. T. (2007). Evaluating protein structures determined by structural genomics consortia. *Proteins*, 66(4), 778–795. <https://doi.org/10.1002/prot.21165>
- Bilsland, E., Bean, D. M., Devaney, E., & Oliver, S. G. (2016). Yeast-based high-throughput screens to identify novel compounds active against *Brugia malayi*. *PLoS Neglected Tropical Diseases*, 10(1), e0004401. <https://doi.org/10.1371/journal.pntd.0004401>
- Brünger, A. T., Adams, P. D., Clore, G. M., DeLano, W. L., Gros, P., Grosse-Kunstleve, R. W., Jiang, J. S., Kuszewski, J., Nilges, M., Pannu, N. S., Read, R. J., Rice, L. M., Simonson, T., & Warren, G. L. (1998). Crystallography & NMR system: A new software suite for macromolecular structure determination. *Acta Crystallographica Section D Biological Crystallography*, 54(Pt 5), 905–921. <https://doi.org/10.1107/s0907444998003254>
- Chandrasekar, R., Sivanesan, S., Natarajan, M., Naveena, K., Preetha, N., Karthika, S., Vimalraj, S., Kron, M., & Dhanasekaran, A. (2021). Evaluation of the angiogenic properties of *Brugia malayi* asparaginyl-tRNA synthetase and its mutants: A study on the molecular target for antifilarial drug development. *Molecular and Biochemical Parasitology*, 246, 111426. <https://doi.org/10.1016/j.molbiopara.2021.111426>
- Crepin, T., Peterson, F., Haertlein, M., Jensen, D., Wang, C., Cusack, S., & Kron, M. (2011). A hybrid structural model of the complete *Brugia malayi* cytoplasmic asparaginyl-tRNA synthetase. *Journal of Molecular Biology*, 405(4), 1056–1069. <https://doi.org/10.1016/j.jmb.2010.11.049>
- Deng, X., Eickholt, J., & Cheng, J. (2012). A comprehensive overview of computational protein disorder prediction methods. *Molecular bioSystems*, 8(1), 114–121. <https://doi.org/10.1039/c1mb05207a>
- Francklyn, C. S., & Mullen, P. (2019). Progress and challenges in aminoacyl-tRNA synthetase-based therapeutics. *The Journal of Biological Chemistry*, 294(14), 5365–5385. <https://doi.org/10.1074/jbc.REV118.002956>
- Gong, Q., & Ishima, R. (2007). 15N-{1H} NOE experiment at high magnetic field strengths. *Journal of Biomolecular NMR*, 37(2), 147–157. <https://doi.org/10.1007/s10858-006-9125-7>
- Guntert, P. (2004). Automated NMR structure calculation with CYANA. *Methods in Molecular Biology*, 278, 353–378. <https://doi.org/10.1385/1-59259-809-9:353>

- Guo, M., Yang, X.-L., & Schimmel, P. (2010). New functions of aminoacyl-tRNA synthetases beyond translation. *Nature Reviews Molecular Cell Biology*, 11(9), 668–674. <https://doi.org/10.1038/nrm2956>
- Howard, O. M. Z., Dong, H. F., De Yang, Y., Raben, N., Nagaraju, K., Rosen, A., Casciola-Rosen, L., Härtle, M., Kron, M., Yang, D., Yiadom, K., Dwivedi, S., Plotz, P. H., & Oppenheim, J. J. (2002). Histidyl-tRNA synthetase and asparaginyl-tRNA synthetase, autoantigens in myositis, activate chemokine receptors on T lymphocytes and immature dendritic cells. *The Journal of Experimental Medicine*, 196(6), 781–791. <https://doi.org/10.1084/jem.20020186>
- Ibba, M., & Söll, D. (2000). Aminoacyl-tRNA synthesis. *Annual Review of Biochemistry*, 69(1), 617–650. <https://doi.org/10.1146/annurev.biochem.69.1.617>
- Ikura, M., Kay, L. E., & Bax, A. (1990). A novel approach for sequential assignment of proton, carbon-13, and nitrogen-15 spectra of larger proteins: Heteronuclear triple-resonance three-dimensional NMR spectroscopy. Application to calmodulin. *Biochemistry*, 29(19), 4659–4667. <https://doi.org/10.1021/bi00471a022>
- Imai, Y. N., Inoue, Y., & Yamamoto, Y. (2007). Propensities of polar and aromatic amino acids in noncovalent interactions: Nonbonded contacts analysis of protein–Ligand complexes in crystal structures. *Journal of Medicinal Chemistry*, 50(6), 1189–1196. <https://doi.org/10.1021/jm061038a>
- Ishida, T., & Kinoshita, K. (2007). PrDOS: Prediction of disordered protein regions from amino acid sequence. *Nucleic Acids Research*, 35(Web Server issue), W460–464. <https://doi.org/10.1093/nar/gkm363>
- Kay, L. E., Ikura, M., Tschudin, R., & Bax, A. (1990). Three-dimensional triple-resonance NMR spectroscopy of isotopically enriched proteins. *Journal of Magnetic Resonance (1969)*, 89(3), 496–514. [https://doi.org/10.1016/0022-2364\(90\)90333-5](https://doi.org/10.1016/0022-2364(90)90333-5)
- Kay, L. E., Torchia, D. A., & Bax, A. (1989). Backbone dynamics of proteins as studied by 15N inverse detected heteronuclear NMR spectroscopy: Application to staphylococcal nuclease. *Biochemistry*, 28(23), 8972–8979. <https://doi.org/10.1021/bi00449a003>
- Kharchenko, V., Nowakowski, M., Jaremko, M., Ejchart, A., & Jaremko, Ł. (2020). Dynamic 15N{1H} NOE measurements: A tool for studying protein dynamics. *Journal of Biomolecular NMR*, 74(12), 707–716. <https://doi.org/10.1007/s10858-020-00346-6>
- Koradi, R., Billeter, M., & Wuthrich, K. (1996). MOLMOL: A program for display and analysis of macromolecular structures. *Journal of Molecular Graphics*, 14(1), 51–55. [https://doi.org/10.1016/0263-7855\(96\)00009-4](https://doi.org/10.1016/0263-7855(96)00009-4)
- Kron, M. A., Jankovic, S. V., Metwali, A., & Elliott, D. (2013). Nematode Asparaginyl-tRNA synthetase resolves intestinal inflammation in mice with T-cell transfer colitis. *Clinical and Vaccine Immunology*, 20(2), 276–281. <https://doi.org/10.1128/CVI.00594-12>
- Kron, M. A., Wang, C., Vodanovic-Jankovic, S., Zack Howard, O. M., & Kuhn, L. A. (2012). Interleukin-8-like activity in a filarial asparaginyl-tRNA synthetase. *Molecular and Biochemical Parasitology*, 185(1), 66–69. <https://doi.org/10.1016/j.molbiopara.2012.06.003>
- Laupland, K. B., & Conly, J. M. (2003). Treatment of staphylococcus aureus colonization and prophylaxis for infection with topical intranasal mupirocin: An evidence-based review. *Clinical Infectious Diseases*, 37(7), 933–938. <https://doi.org/10.1086/377735>
- Liu, F., Cheng, W., Pappoe, F., Hu, X., Wen, H., Luo, Q., Wang, S., Deng, F., Xie, Y., Xu, Y., & Shen, J. (2016). Schistosoma japonicum cystatin attenuates murine collagen-induced arthritis. *Parasitology Research*, 115(10), 3795–3806. <https://doi.org/10.1007/s00436-016-5140-0>
- Liu, F., Cui, S. J., Hu, W., Feng, Z., Wang, Z. Q., & Han, Z. G. (2009). Excretory/secretory proteome of the adult developmental stage of human blood fluke, *Schistosoma japonicum*. *Molecular & Cellular Proteomics*, 8(6), 1236–1251. <https://doi.org/10.1074/mcp.M800538-MCP200>
- Liu, Y., Wang, X., & Liu, B. (2019). A comprehensive review and comparison of existing computational methods for intrinsically disordered protein and region prediction. *Briefings in Bioinformatics*, 20(1), 330–346. <https://doi.org/10.1093/bib/bbx126>
- Maizels, R. M. P., & McSorley, H. J. P. (2016). Regulation of the host immune system by helminth parasites. *The Journal of Allergy and Clinical Immunology*, 138(3), 666–675. <https://doi.org/10.1016/j.jaci.2016.07.007>
- Maizels, R. M., Smits, H. H., & McSorley, H. J. (2018). Modulation of host immunity by helminths: The expanding repertoire of parasite effector molecules. *Immunity*, 49(5), 801–818. <https://doi.org/10.1016/j.immuni.2018.10.016>
- Marley, J., Lu, M., & Bracken, C. (2001). A method for efficient isotopic labeling of recombinant proteins. *Journal of Biomolecular NMR*, 20(1), 71–75. <https://doi.org/10.1023/A:1011254402785>
- Meng, F., Uversky, V. N., & Kurgan, L. (2017). Comprehensive review of methods for prediction of intrinsic disorder and its molecular functions. *Cellular and Molecular Life Sciences : CMLS*, 74(17), 3069–3090. <https://doi.org/10.1007/s00018-017-2555-4>
- Meng, F., Uversky, V., & Kurgan, L. (2017). Computational prediction of intrinsic disorder in proteins. *Current Protocols in Protein Science*, 88, 2.16.1–2.16.14. <https://doi.org/10.1002/cpps.28>
- Mobli, M., Maciejewski, M. W., Gryk, M. R., & Hoch, J. C. (2007). An automated tool for maximum entropy reconstruction of biomolecular NMR spectra. *Nature Methods*, 4(6), 467–468. <https://doi.org/10.1038/nmeth0607-467>
- Monastyrskyy, B., Kryshtafovych, A., Moutl, J., Tramontano, A., & Fidelis, K. (2014). Assessment of protein disorder region predictions in CASP10. *Proteins*, 82(2), 127–137. <https://doi.org/10.1002/prot.24391>
- Nederveen, A. J., Doreleijers, J. F., Vranken, W., Miller, Z., Spronk, C. A., Nabuurs, S. B., Güntert, P., Livny, M., Markley, J. L., Nilges, M., Ulrich, E. L., Kaptein, R., & Bonvin, A. M. (2005). RECOORD: A recalculated coordinate database of 500+ proteins from the PDB using restraints from the BioMagResBank. *Proteins*, 59(4), 662–672. <https://doi.org/10.1002/prot.20408>
- Nutman, T. B. (2015). Looking beyond the induction of Th2 responses to explain immunomodulation by helminths. *Parasite Immunology*, 37(6), 304–313. <https://doi.org/10.1111/pim.12194>
- Nyamai, D. W., & Tasthan Bishop, Ö. (2019). Aminoacyl tRNA synthetases as malarial drug targets: A comparative bioinformatics study. *Malaria Journal*, 18(1), 34. <https://doi.org/10.1186/s12936-019-2665-6>
- O'Dwyer, K., Spivak, A. T., Ingraham, K., Min, S., Holmes, D. J., Jakielaszek, C., Rittenhouse, S., Kwan, A. L., Livi, G. P., Sathe, G., Thomas, E., Horn, S. V., Miller, L. A., Twynholm, M., Tomayko, J., Dalessandro, M., Caltabiano, M., Scangarella-Oman, N. E., & Brown, J. R. (2015). Bacterial resistance to Leucyl-tRNA synthetase inhibitor GSK2251052 develops during treatment of complicated urinary tract infections. *Antimicrobial Agents and Chemotherapy*, 59(1), 289–298. <https://doi.org/10.1128/AAC.03774-14>
- Orabi, E. A., & English, A. M. (2016). Sulfur-aromatic interactions: Modeling cysteine and methionine binding to tyrosinate and histidinium ions to assess their influence on protein electron transfer. *Israel Journal of Chemistry*, 56(9–10), 872–885. <https://doi.org/10.1002/ijch.201600047>
- Palmer, A. G. (1997). Probing molecular motion by NMR. *Current Opinion in Structural Biology*, 7(5), 732–737. [https://doi.org/10.1016/S0959-440X\(97\)80085-1](https://doi.org/10.1016/S0959-440X(97)80085-1)
- Pang, Y. L. J., Poruri, K., & Martinis, S. A. (2014). tRNA synthetase: TRNA aminoacylation and beyond. *Wiley Interdisciplinary Reviews. RNA*, 5(4), 461–480. <https://doi.org/10.1002/wrna.1224>
- Park, J. S., Park, M. C., Lee, K.-Y., Goughnour, P. C., Jeong, S. J., Kim, H. S., Kim, H.-J., Lee, B.-J., Kim, S., & Han, B. W. (2018). Unique N-terminal extension domain of human asparaginyl-tRNA synthetase elicits CCR3-mediated chemokine activity. *International Journal of Biological Macromolecules*, 120(Pt A), 835–845. <https://doi.org/10.1016/j.ijbiomac.2018.08.171>
- Pham, J. S., Dawson, K. L., Jackson, K. E., Lim, E. E., Pasaje, C. F. A., Turner, K. E. C., & Ralph, S. A. (2014). Aminoacyl-tRNA synthetases as drug targets in eukaryotic parasites. *International Journal for Parasitology. Drugs and Drug Resistance*, 4(1), 1–13. <https://doi.org/10.1016/j.ijpddr.2013.10.001>
- Rahnama, S., Deus, J. R., Cardoso, F. C., Ramanujam, V., Lewis, R. J., Rash, L. D., King, G. F., Vetter, I., & Mobli, M. (2017). The structure, dynamics and selectivity profile of a NaV1.7 potency-optimised huwentoxin-IV variant. *PLoS One*, 12(3), e0173551. <https://doi.org/10.1371/journal.pone.0173551>

- Rajendran, V., Shukla, R., Shukla, H., & Tripathi, T. (2018). Structure-function studies of the asparaginyl-tRNA synthetase from *Fasciola gigantica*: Understanding the role of catalytic and non-catalytic domains. *The Biochemical Journal*, 475(21), 3377–3391. <https://doi.org/10.1042/bcj20180700>
- Ramirez, B. L., Howard, O. M. Z., Dong, H. F., Edamatsu, T., Gao, P., Hartlein, M., & Kron, M. (2006). *Brugia malayi* asparaginyl-transfer RNA synthetase induces chemotaxis of human leukocytes and activates G-protein-coupled receptors CXCR1 and CXCR2. *The Journal of Infectious Diseases*, 193(8), 1164–1171. <https://doi.org/10.1086/501369>
- Randall, C. P., Rasina, D., Jirgensons, A., & O'Neill, A. J. (2016). Targeting multiple aminoacyl-tRNA synthetases overcomes the resistance liabilities associated with antibacterial inhibitors acting on a single such enzyme. *Antimicrobial Agents and Chemotherapy*, 60(10), 6359–6361. <https://doi.org/10.1128/AAC.00674-16>
- Rock, F. L., Mao, W., Yaremchuk, A., Tukalo, M., Crépin, T., Zhou, H., Zhang, Y.-K., Hernandez, V., Akama, T., Baker, S. J., Plattner, J. J., Shapiro, L., Martinis, S. A., Benkovic, S. J., Cusack, S., & Alley, M. R. K. (2007). An antifungal agent inhibits an aminoacyl-tRNA synthetase by trapping tRNA in the editing site. *Science (New York, N.Y.)*, 316(5832), 1759–1761. <https://doi.org/10.1126/science.1142189>
- Ryan, S. M., Eichenberger, R. M., Ruscher, R., Giacomini, P. R., & Loukas, A. (2020). Harnessing helminth-driven immunoregulation in the search for novel therapeutic modalities. *PLoS Pathogens*, 16(5), e1008508. <https://doi.org/10.1371/journal.ppat.1008508>
- Saez, N. J., Mobli, M., Bieri, M., Chassagnon, I. R., Malde, A. K., Gamsjaeger, R., Mark, A. E., Gooley, P. R., Rash, L. D., & King, G. F. (2011). A dynamic pharmacophore drives the interaction between Psalmitoxin-1 and the putative drug target acid-sensing ion channel 1a. *Molecular Pharmacology*, 80(5), 796–808. <https://molpharm.aspet-journals.org/content/80/5/796.long> <https://doi.org/10.1124/mol.111.072207>
- Saint-Léger, A., Sinadinos, C., & Ribas de Pouplana, L. (2016). The growing pipeline of natural aminoacyl-tRNA synthetase inhibitors for malaria treatment. *Bioengineered*, 7(2), 60–64. <https://doi.org/10.1080/21655979.2016.1149270>
- Shan, W., Zhang, W., Xue, F., Ma, Y., Dong, L., Wang, T., Zheng, Y., Feng, D., Chang, M., Yuan, G., & Wang, X. (2021). Schistosoma japonicum peptide SJMHE1 inhibits acute and chronic colitis induced by dextran sulfate sodium in mice. *Parasites & Vectors*, 14(1), 455. <https://doi.org/10.1186/s13071-021-04977-y>
- Shen, Y., & Bax, A. (2013). Protein backbone and sidechain torsion angles predicted from NMR chemical shifts using artificial neural networks. *Journal of Biomolecular NMR*, 56(3), 227–241. <https://doi.org/10.1007/s10858-013-9741-y>
- Shen, Y., Delaglio, F., Cornilescu, G., & Bax, A. (2009). TALOS+: A hybrid method for predicting protein backbone torsion angles from NMR chemical shifts. *Journal of Biomolecular NMR*, 44(4), 213–223. <https://doi.org/10.1007/s10858-009-9333-z>
- Smallwood, T. B., Giacomini, P. R., Loukas, A., Mulvenna, J. P., Clark, R. J., & Miles, J. J. (2017). Helminth immunomodulation in autoimmune disease. *Frontiers in Immunology*, 8, 453–453. <https://doi.org/10.3389/fimmu.2017.00453>
- Sun, X., Liu, Y. H., Lv, Z. Y., Yang, L. L., Hu, S. M., Zheng, H. Q., Hu, W., Cao, J. P., Fung, M. Q., & Wu, Z. D. (2010). rSj16, a recombinant protein of *Schistosoma japonicum*-derived molecule, reduces severity of the complete Freund's adjuvant-induced adjuvant arthritis in rats' model. *Parasite Immunology*, 32(11–12), 739–748. <https://doi.org/10.1111/j.1365-3024.2010.01240.x>
- Valley, C. C., Cembran, A., Perlmutter, J. D., Lewis, A. K., Labello, N. P., Gao, J., & Sachs, J. N. (2012). The methionine-aromatic motif plays a unique role in stabilizing protein structure [Article]. *The Journal of Biological Chemistry*, 287(42), 34979–34991. <https://doi.org/10.1074/jbc.M112.374504>
- Vranken, W. F., Boucher, W., Stevens, T. J., Fogh, R. H., Pajon, A., Llinas, M., Ulrich, E. L., Markley, J. L., Ionides, J., & Laue, E. D. (2005). The CCPN data model for NMR spectroscopy: Development of a software pipeline. *Proteins*, 59(4), 687–696. <https://doi.org/10.1002/prot.20449>
- Wang, X., Li, L., Wang, J., Dong, L., Shu, Y., Liang, Y., Shi, L., Xu, C., Zhou, Y., Wang, Y., Chen, D., & Mao, C. (2017). Inhibition of cytokine response to TLR stimulation and alleviation of collagen-induced arthritis in mice by *Schistosoma japonicum* peptide SJMHE1. *Journal of Cellular and Molecular Medicine*, 21(3), 475–486. <https://doi.org/10.1111/jcmm.12991>
- Wang, L. F., Xie, H., Xu, L., Liao, Q., Wan, S., Yu, Z. L., Lin, D. T., Zhang, B. B., Lv, Z. Y., Wu, Z. D., & Sun, X. (2017). rSj16 protects against DSS-induced colitis by inhibiting the PPAR-alpha signaling pathway. *Theranostics*, 7(14), 3446–3460. <https://doi.org/10.7150/thno.20359>
- Wishart, D. S., Bigam, C. G., Holm, A., Hodges, R. S., & Sykes, B. D. (1995). <sup>1</sup>H, <sup>13</sup>C and <sup>15</sup>N random coil NMR chemical shifts of the common amino acids. I. Investigations of nearest-neighbor effects. *Journal of Biomolecular NMR*, 5(1), 67–81. <https://doi.org/10.1007/bf00227471>
- Yang, X.-L. (2013). Structural disorder in expanding the functionome of aminoacyl-tRNA synthetases. *Chemistry & Biology*, 20(9), 1093–1099. <https://doi.org/10.1016/j.chembiol.2013.07.013>
- Zhang, W., Li, L., Zheng, Y., Xue, F., Yu, M., Ma, Y., Dong, L., Shan, Z., Feng, D., Wang, T., & Wang, X. (2019). Schistosoma japonicum peptide SJMHE1 suppresses airway inflammation of allergic asthma in mice. *Journal of Cellular and Molecular Medicine*, 23(11), 7819–7829. <https://doi.org/10.1111/jcmm.14661>
- Zhou, J., Oldfield, C. J., Yan, W., Shen, B., & Dunker, A. K. (2019). Intrinsically disordered domains: Sequence → disorder → function relationships. *Protein Science*, 28(9), 1652–1663. <https://doi.org/10.1002/pro.3680>
- Zhou, H.-X., & Pang, X. (2018). Electrostatic interactions in protein structure, folding, binding, and condensation. *Chemical Reviews*, 118(4), 1691–1741. <https://doi.org/10.1021/acs.chemrev.7b00305>